ADVANCED FUNCTIONAL MATERIALS
www.afm-journal.de

Materials Views
www.MaterialsViews.com

Incipient Ferroelectricity in Al-Doped HfO_2 Thin Films

Stefan Mueller, Johannes Mueller, Aarti Singh, Stefan Riedel, Jonas Sundqvist, Uwe Schroeder, and Thomas Mikolajick*

Incipient ferroelectricity is known to occur in perovskites such as $SrTiO_3$, $KTaO_3$, and $CaTiO_3$. For the first time it is shown that the intensively researched HfO_2 thin films (16 nm) also possess ferroelectric properties when aluminium is incorporated into the host lattice. Polarization measurements on Al:HfO_2 based metal–insulator–metal capacitors show an antiferroelectric-to-ferroelectric phase transition depending on annealing conditions and aluminium content. Structural investigation of the electrically characterized capacitors by grazing incidence X-ray diffraction is presented in order to gain further insight on the potential origin of ferroelectricity. The non-centrosymmetry of the elementary cell, which is essential for ferroelectricity, is assumed to originate from an orthorhombic phase of space group $Pbc2_1$ stabilized for low Al doping in HfO_2. The ferroelectric properties of the modified HfO_2 thin films yield high potential for various ferroelectric, piezoelectric, and pyroelectric applications. Furthermore, due to the extensive knowledge accumulated by various research groups regarding the HfO_2 dielectric, an immediate relevance of ferroelectric hafnium oxide thin films is anticipated by the authors.

1. Introduction

The most prominent examples for incipient ferroelectrics are strontium and calcium titanate as well as potassium tantalate which, as bulk materials, maintain their paraelectric properties down to temperatures close to absolute zero.[1–3] Hence, incipient ferroelectric materials are actually paraelectric in the first place; however, a ferroelectric phase can be stabilized under certain conditions. Mechanical confinement,[4] doping,[5] defects,[6] stoichiometry variations,[7] or exchange of (oxygen) isotopes[8] have been shown to induce ferroelectricity for previously paraelectric materials.[9] Hence, the originally paraelectric phase, which is assumed to be stabilized by quantum fluctuations,[10] transforms to a ferroelectric phase. For $SrTiO_3$ thin films in particular, ferroelectricity can be provoked by mechanical stress[4] caused by lattice mismatches between thin film and substrate. The above-mentioned stabilization conditions affect the thermodynamic free energy and can therefore contribute to a ferroelectric phase formation. A theoretical description of this free energy modification is given by Landau–Ginzburg–Devonshire theory.[11] It is plausible that mechanical stress can influence ferroelectric phases in thin films, since it already affects bulk ferroelectrictiy significantly.[12,13]

As previous studies have shown, incipient ferroelectricity not only exists for ABO_3-type perovskite materials but is also anticipated for oxides such as TiO_2.[14–16] Only recently, ferroelectricity for HfO_2 was discovered for the first time.[17–19] The authors showed that doping HfO_2 thin films with silicon, zirconium, or yttrium combined with an additional annealing step induces a crystalline phase that has (anti-)ferroelectric characteristics. Hence, hafnium oxide represents an additional compound belonging to the class of incipient ferroelectrics.

In this study we show for the first time that, by using trivalent aluminium, which is smaller than hafnium in terms of atomic radius, as a cation-substituting species within the HfO_2 lattice, it is possible to induce ferroelectricity without the support of a mechanically confining top electrode. From an application point of view, these findings are of significant importance since they eliminate the perception that it is only possible to induce ferroelectricity in uncapped HfO_2 by using rare-earth dopants like yttrium.

We support our findings with polarization measurements as well as by the identification of a possibly orthorhombic phase of space group $Pbc2_1$, whose non-centrosymmetry would explain the origin of ferroelectricity.

S. Mueller, Dr. A. Singh, Dr. U. Schroeder, Prof. T. Mikolajick
NaMLab gGmbH
Dresden University of Technology
Noethnitzerstraße 64, 01187 Dresden, Germany
E-mail: stefan.mueller@namlab.com
J. Mueller, S. Riedel, Dr. J. Sundqvist
Fraunhofer Center Nanoelectronic Technologies
Koenigsbrueckerstraße 180, 01099 Dresden, Germany

DOI: 10.1002/adfm.201103119

2. Results and Discussion

Metal–insulator–metal (MIM) capacitors were manufactured in order to investigate the electrical properties of the Al:HfO_2 thin films. The thin film layers were formed on a highly doped silicon substrate in order to allow for a low resistive backside contact during electrical measurements. First, an approximately 12 nm TiN bottom electrode was deposited by pulsed chemical vapor deposition (CVD) at 450 °C. The 16 nm Al:HfO_2 layer

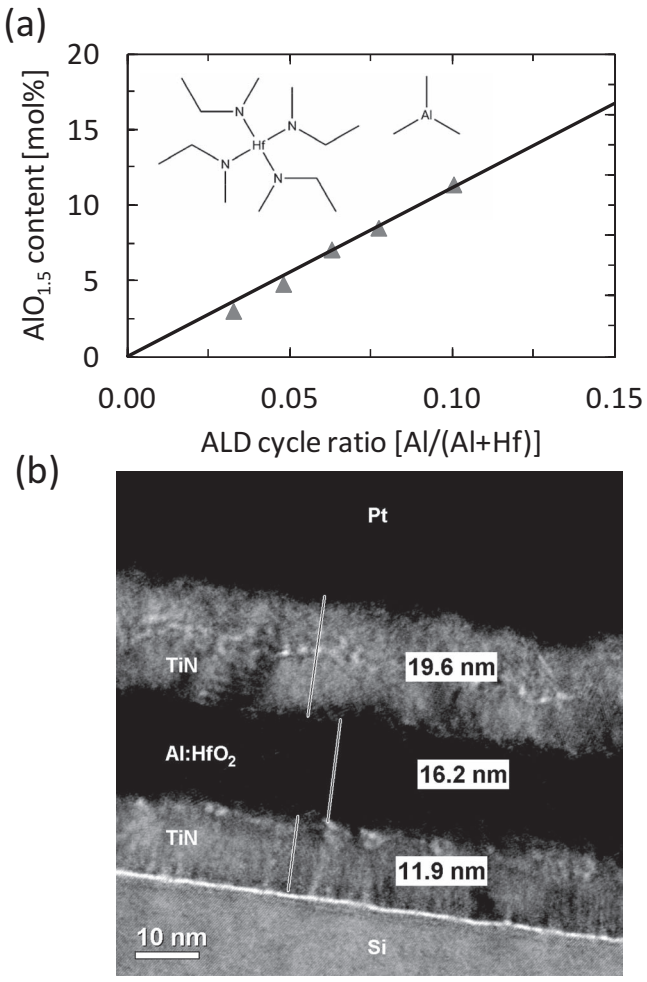

Figure 1. a) Incorporated $AlO_{1.5}$ content within the HfO_2 host lattice according to XPS characterization. Using tetrakis(ethylmethylamino)hafnium and trimethylaluminium (chemical formulae shown as inset) for ALD deposition, an almost ideal linear behavior could be achieved for the chosen cycle ratios. b) EM image of an MIM capacitor used within these studies. The structure consists of a platinum contact situated on top of the aluminium-doped HfO_2 sandwiched between TiN electrodes. Even though a hydrogen fluoride dip was used before bottom electrode formation, a very thin amorphous interface is still visible (bright interface between TiN and Si).

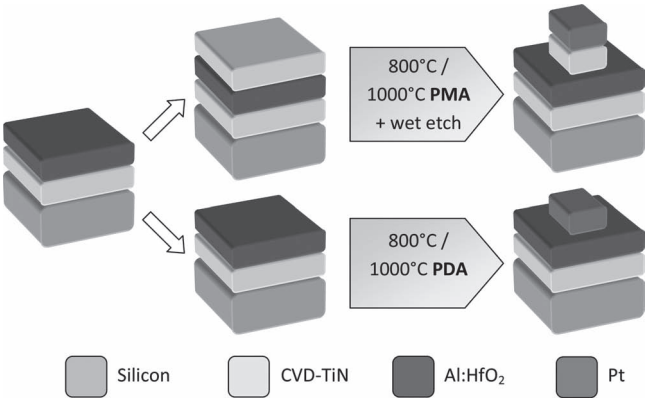

Figure 2. PMA versus PDA process flow. For the PMA samples, a CVD-TiN top electrode is deposited which creates an additional mechanical confinement of the aluminium-doped HfO_2. The PMA process flow uses the platinum contact as a hard mask for etching the TiN top electrode.

was deposited afterwards by atomic layer deposition (ALD, 300°C substrate temperature). Different ALD supercycles of the precursor gases (see the Experimental Section) were used in order to realize various molar concentrations of aluminium within the HfO_2 lattice. An almost ideal linear relationship between molar percentage of aluminium in HfO_2 and cycle ratio could be achieved, which indicates a very controlled deposition process (**Figure 1**a). A TiN top electrode of approximately 20 nm thickness was deposited on top of the hafnium oxide again using pulsed CVD (450 °C). After top electrode formation, samples were exposed to rapid thermal annealing (RTA) for either 20 s at 800 °C or for 1 s at 1000 °C in a nitrogen environment. In the following, these samples will be abbreviated PMA samples (post-metallization annealing) since the annealing step was performed after the TiN top electrode had been deposited. Finally, platinum contacts were formed by physical vapor deposition (evaporation) using a shadow mask. The layout of the shadow mask was such as to deposit platinum dot sizes of 110, 200, 280, and 450 µm in diameter. The platinum dots were also used as a hard mask for wet chemical etching of the TiN top electrode down to the Al:HfO_2 layer. The quality of deposition and annealing processes was investigated by transmission electron microscopy (TEM, Figure 1b). The polycrystalline nature of both electrodes and the Al:HfO_2 thin film is shown for a 1000 °C PMA sample. Furthermore, for another batch of samples, the formation of a TiN top electrode was omitted and the platinum contacts were deposited directly on top of the Al:HfO_2 thin film. Since the annealing step was performed after the dielectric/ferroelectric layer formation, these samples will be abbreviated PDA samples (post-deposition annealing). The process flow for PMA and PDA samples is summarized in **Figure 2**.

The surface morphology and the quality of the Al:HfO_2 thin film was characterized by atomic force microscopy (AFM; **Figure 3**). The root mean square (RMS) surface roughness of the PMA samples is significantly smaller than for the PDA samples. Hence, the vertical grain growth during annealing is homogenized by depositing a TiN cap between platinum contact and the doped hafnium oxide. Moreover, an increased surface roughness was also reflected by the leakage current and breakdown characteristics of the capacitors, i.e., the PDA process led to increased leakage currents and smaller breakdown voltages. The effects of TiN capping have been extensively investigated for pure HfO_2, with similar conclusions being reached.[20]

Polarization measurements were performed in order to investigate a potential hysteretic behavior of *P*–*E* characteristics (**Figure 4**). By applying a triangular AC voltage signal to the samples, a ferroelectric capacitor would switch into the respective polarization state. The written state can only be reversed if a certain voltage (larger than the coercive voltage) of opposite polarity is again applied to the capacitor.

Large amounts of aluminium inside the host lattice lead to antiferroelectric polarization loops. The antiferroelectric phase might be considered a relaxor phase, in which ferroelectric

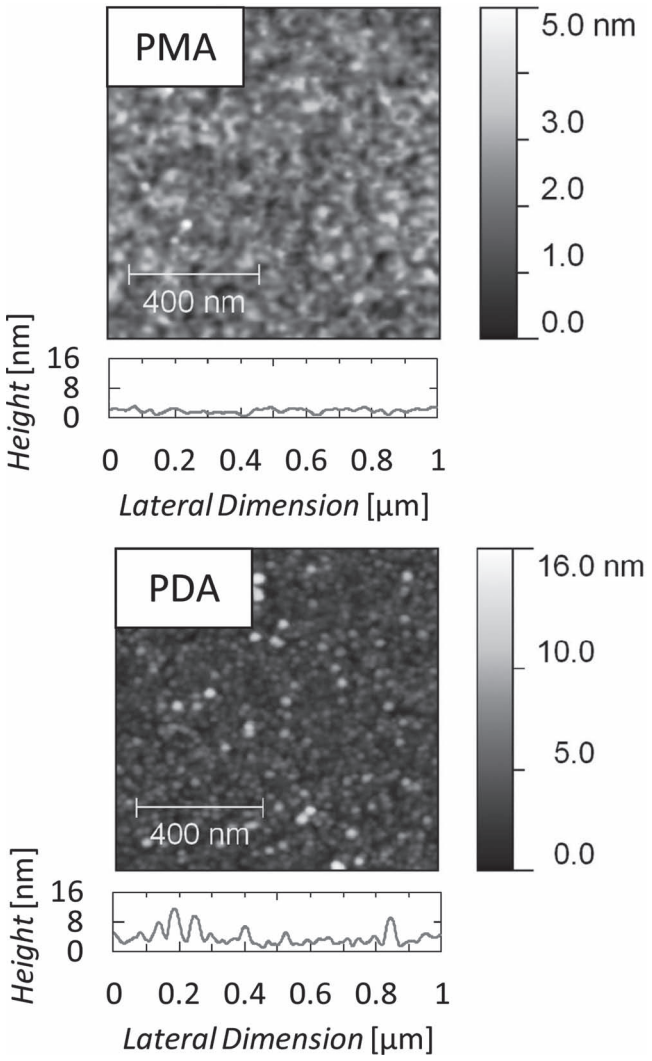

Figure 3. AFM RMS surface roughness measurements for PMA and PDA samples. Both graphs were measured directly on the surface of the ferroelectric, i.e., in between the structured MIM capacitors. The mechanical confinement of the TiN top electrode significantly reduces the surface roughness.

clusters of different polarization directions exist within a paraelectric matrix.[21] However, by reducing the aluminium content, the antiferroelectric behavior transforms to ferroelectric characteristics (Figure 4a). Molar concentrations of 4.8% show saturated ferroelectric responses having remanent polarizations of around 5 µC cm^{-2} and coercive fields of approximately 1 MV cm^{-1}.

Remarkably, omitting the TiN top electrode does not inhibit ferroelectricity (Figure 4b) as it is the case in silicon-doped hafnium oxide.[17] Even though the remanent polarization is reduced, a ferroelectric hysteresis loop is clearly observable for PDA-samples. Furthermore, ferroelectricity seems to be more pronounced for samples which are annealed at higher temperatures (Figure 4c). It is noteworthy that already the as-deposited sample having 7.1 mol% aluminium concentration shows antiferroelectric tendency. At 1000 °C PMA the ferroelectric behavior is most pronounced.

Generally, dielectric permittivity increases for higher aluminium contents and shows a maximum for antiferroelectric capacitors (Figure 4d). However, compared to traditional ferroelectrics like lead zirconate titanate ($Pb[Zr_xTi_{1-x}]O_3$; PZT), which can possess relative permittivities even above 200, the tendency for dielectric polarization is significantly smaller for doped hafnium oxide. Furthermore, it is interesting to see that the highest remanent polarization is actually achieved for samples with 7.1 mol% aluminium content even though the polarization loops are not as ideal as for samples having 4.8 mol% incorporation of aluminium (compare Figure 4a,c). This again indicates that, for this composition, the capacitors possess antiferroelectric as well as ferroelectric domains.

In order to prove that the ferroelectric behavior might not only be field induced, the crystal structures of the samples were physically characterized using grazing incidence X-ray diffraction analysis (GI-XRD). The acquired diffractograms were used to identify the respective crystalline phases, as well as non-centrosymmetric phase which would be responsible for the ferroelectric phenomena (**Figure 5**a).

Under atmospheric pressure and increasing temperature, hafnium oxide transforms from a monoclinic to a tetragonal and finally to a cubic lattice structure.[22] However, it has been shown that the tetragonal and cubic phases in HfO_2 and ZrO_2 can be stabilized by incorporation of nano-crystallites and nitrogen respectively.[23,24] For the material system at hand, the acquired X-ray diffraction patterns show that, for increasing aluminium concentration, a transition from the monoclinic phase towards a cubic lattice structure occurs. That is, the cubic phase is stabilized if aluminium is used as a substituting element. This stabilization can best be observed in the interval between 80° and 90° where the monoclinic peaks observed for pure HfO_2 convert into two sharp reflections, which are characteristic of the cubic phase. For 4.8 mol% aluminium the diffractogram is compared to the diffraction pattern of a previously derived non-centrosymmetric orthorhombic phase of space group $Pbc2_1$.[17] This phase was originally derived from manganese-stabilized zirconium oxide[25,26] since all known orthorhombic phases for HfO_2 are centrosymmetric (space groups Pbca and Pbcm). The non-centrosymmetric orthorhombic phase of space group $Pbc2_1$ is assumed to be applicable also to the HfO_2 host lattice when isotropic rescaling is applied.[17] It is however difficult to unambiguously identify the existence of this phase, since there is no peak which is unique to the orthorhombic phase. Peaks which appear to be unique for the orthorhombic phase overlap with reflections originating from the TiN top and bottom electrodes at 36.7°, 42.6°, and 61.8°. However, the existence of the orthorhombic phase seems justified if the reflections in the interval between 80° and 90° (Figure 5b) are analyzed. Simply superimposing monoclinic and cubic diffraction patterns will not yield reflections observed for 4.8 mol% of aluminium concentration. Hence, there has to be a non-centrosymmetric transition phase since this is a prerequisite for the ferroelectric characteristics observed in electrical measurements. In summary, the authors suggest the existence of an orthorhombic phase of space group $Pbc2_1$ causing the ferroelectric nature of Al:HfO_2.

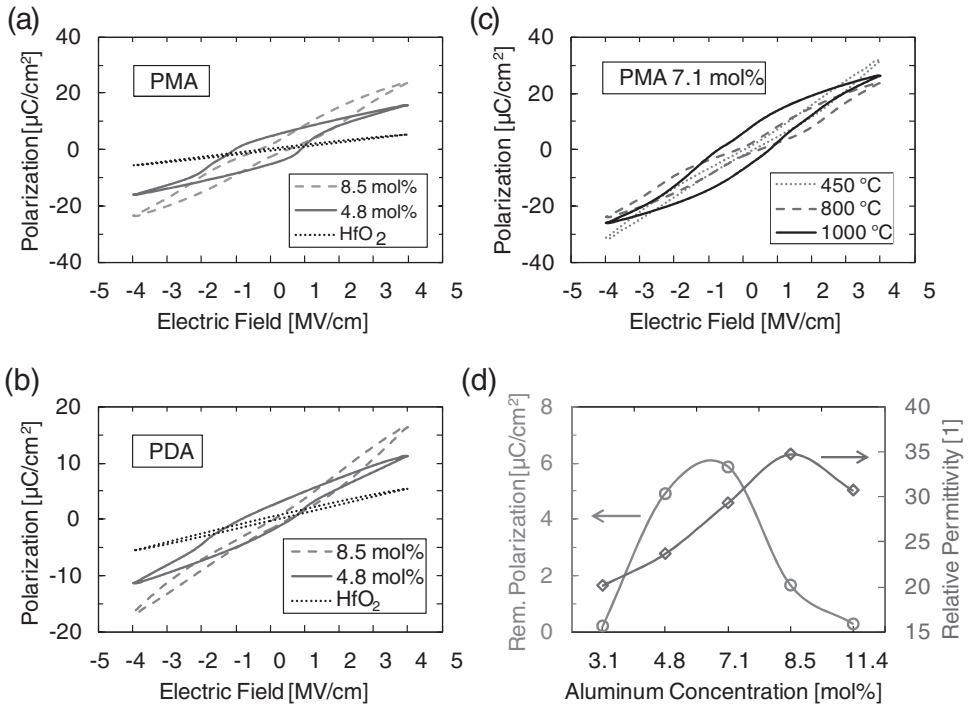

Figure 4. a) Polarization hysteresis for PMA samples annealed at 1000°C for 20 s. Decreasing aluminium concentration yields an antiferroelectric-to-ferroelectric transition whereas the pure hafnium oxide is paraelectric, as expected. b) Polarization hysteresis for PDA samples annealed at 1000 °C for 20 s. The same antiferroelectric-to-ferroelectric transition as for the PMA samples can be observed but the remanent polarization is significantly lower. c) Polarization hysteresis of a HfO_2 MIM capacitor with 7.1 mol% of incorporated aluminium for different annealing temperatures. A transition towards ferroelectric behavior can be observed if higher temperatures are used for the PMA. d) Remanent polarization and relative permittivity versus amount of incorporated aluminium for PMA capacitors annealed at 1000 °C for 20 s.

3. Conclusions

Thin films of aluminium-doped HfO_2 of 16 nm thickness were investigated. Electrical characterization showed the incipient antiferroelectric and ferroelectric nature of the material system due to the incorporation of aluminium into the host lattice. Electrical permittivities reached maximum values of around 35 for samples in which antiferroelectricity had been provoked. GI-XRD analysis indicated that the necessary non-centrosymmetry of the elementary cell can most likely be assigned to an orthorhombic $Pbc2_1$ phase located in the vicinity of the transition from purely monoclinic HfO_2 to the cubic lattice of highly doped HfO_2.

The recently discovered ferroelectric properties of this material system are advantageous not only because of the extensive industrial expertise regarding HfO_2-based dielectrics but also because of the CMOS-integratability of both hafnium oxide and aluminium. The authors anticipate that HfO_2 ferroelectric thin films of only 16 nm thickness might be of interest to various research and industry communities, especially because its properties are highly tunable (through the doping concentration, annealing conditions, and mechanical confinement). Applications like ferroelectric random access memories, piezoelectric applications or ferroelectric field effect transistors[27–30] might be envisioned. Furthermore, the fact that all ferroelectric materials show pyroelectric as well as piezoelectric properties[31] extends the area of potential applications. The ferroelectricity of HfO_2 might also help in advancing novel electronic devices, like negative capacitance field-effect transistors.[32,33] Moreover, the fact that ferroelectricity can be provoked at annealing temperatures of up to 1000 °C demonstrates the viability for a wide range of applications.

4. Experimental Section

The fabrication and characterization of the Pt/TiN/Al:HfO_2/TiN capacitor stack investigated within this study will be described in the following. A JEL Eureka single wafer ALD reactor was used for manufacturing the ferroelectric layers, whereas TiN top and bottom electrodes were deposited in an ASM A412 batch furnace. The annealing steps were performed using a single wafer Mattson RTP tool. Platinum dots were deposited in a Bestec/Ferrotec EVM6 evaporation chamber. Physical characterization was performed using a Bruker D8 Discover X-ray diffractometer and a Veeco Dimension 3100 AFM. The *P–E* hysteresis measurements were obtained on an Aixacct TF Analyzer 1000.

Atomic Layer Deposition: Aluminium-doped HfO_2 thin films were deposited by atomic layer deposition on 300 mm Si substrates. The silicon substrate received a HF clean in order to minimize the native oxide thickness between substrate and bottom electrode. Prior to dielectric deposition, the 12 nm bottom electrode was chemically vapor deposited ($TiCl_4/NH_3$) in a batch furnace. The ALD process was based on the commercially available metal organic precursors tetrakis(ethylmethylamino)hafnium (TEMAH) and trimethylaluminium (TMA). Ozone was used as the oxidant and argon as the purge and carrier gas. The Al_2O_3 content in HfO_2 ranged from 3.1 to 11.4 mol-% and was defined by varying the cycle ratio of the metal precursors and

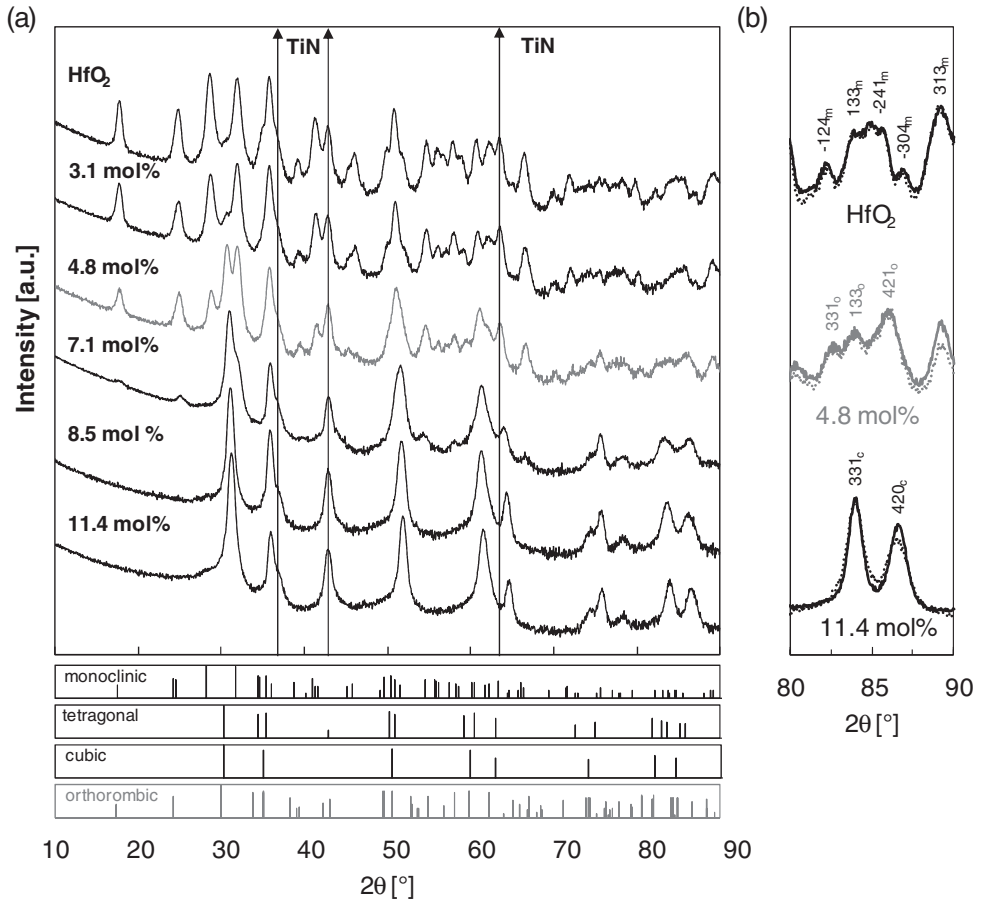

Figure 5. a) GI-XRD diffractograms for PMA samples having different aluminium concentrations. A monoclinic-to-cubic phase transition is clearly visible for increasing aluminium content. The powder diffraction patterns as well as the calculated orthorhombic $Pbc2_1$ reference pattern are shown below the diffractograms. The composition which possesses the purest ferroelectric properties is highlighted in blue. b) Enlarged 2θ scans from 80° to 90° for paraelectric HfO_2 containing no aluminium, ferroelectric HfO_2 containing 4.8 mol% aluminium, and, again, paraelectric HfO_2 containing 11.8 mol% aluminium. The diffractogram of the ferroelectric composition shows a triplet which would not be expected for monoclinic, tetragonal, or cubic phases. The dotted lines show results for PDA samples of the same composition.

monitored by inline X-ray photoelectron spectroscopy (XPS). A constant thickness of 16 nm for all films was achieved by adjusting the number of Hf:Al super cycles, and was confirmed by inline spectral ellipsometry and high resolution transmission electron microscopy (HR-TEM). Crystallization of the as deposited amorphous Al:HfO_2 thin films was induced by a 800 °C/20 s/N_2 or 1000 °C/20 s/N_2 rapid thermal annealing (RTA) step, referred to in the text as PDA. Samples annealed after chemical vapor deposited 20 nm TiN top electrode are referred to in the text as samples treated with PMA.

GI-XRD Characterization: Since a thin film capacitor stack was used for our study, XRD characterization was performed under very small incident angles (grazing incidence). An incident angle of 0.45° was found to yield the highest intensity reflections for pure HfO_2 and was used for all measurements described. Furthermore, a Göbel mirror and a 0.2 mm slit were used on the primary side and a Soller mount on the detector side. For acquisition of the diffractograms, an integration time of 35 s per step and an angular resolution of 0.05° were chosen for the 10° to 90° interval of 2θ. For additional measurements in the interval 80° to 90°, the integration time was increased to 250 s. Separate samples without platinum dots were used for each of the acquired diffractograms.

Electrical Characterization: The polarization versus electric field measurements were derived from integrating the displacement current for an applied triangular AC voltage signal using a virtual ground amplifier (Aixacct TF Analyzer 1000). Capacitors of 200 µm diameter were used for all measurements and a current range of 100 µA provided the best signal-to-noise ratio. A frequency of 1 kHz was used for hysteresis measurements with amplitudes ranges of 4.8, 5.6, and 6.4 V in order to produce electric fields of 3, 3.5, and 4 MV cm^{-1}. Before carrying out any type of electrical characterization, the samples were cycled at least 1000 times in order to provide reproducible switching behavior. Even though leakage currents can also be incorporated in a hysteresis measurement, a dynamic leakage current compensation (DLCC)[34] showed that the leakage currents during *P–E* measurements were negligible.

Acknowledgements

D. Martin is acknowledged for AFM images. The authors would like to thank Dr. U. Böttger for helpful discussions and Prof. A. Kersch for graphical illustrations. The work for this paper was supported within the scope of technology development by the EFRE fund of the European Community and by funding from the Free State of Saxony (Project HEIKO). The authors are responsible for the content of the paper.

Received: December 22, 2011
Published online: March 15, 2012

[1] K. A. Muller, H. Burkard, *Phys. Rev. B* **1979**, *19*, 3593.
[2] A. R. Akbarzadeh, L. Bellaiche, K. Leung, J. Iniguez, D. Vanderbilt, *Phys. Rev. B* **2004**, *70*, 54103/1.
[3] V. V. Lemanov, A. V. Sotnikov, E. P. Smirnova, M. Weihnacht, R. Kunze, *Solid State Commun.* **1999**, *110*, 611.
[4] J. H. Haeni, P. Irvin, W. Chang, R. Uecker, P. Reiche, Y. L. Li, S. Choudhury, W. Tian, M. E. Hawley, B. Craigo, A. K. Tagantsev, X. Q. Pan, S. K. Streiffer, L. Q. Chen, S. W. Kirchoefer, J. Levy, D. G. Schlom, *Nature* **2004**, *430*, 758.
[5] T. Mitsui, W. B. Westphal, *Phys. Rev.* **1961**, *124*, 1354.
[6] Y. S. Kim, D. J. Kim, T. H. Kim, T. W. Noh, J. S. Choi, B. H. Park, J. G. Yoon, *Appl. Phys. Lett.* **2007**, *91*, 42908/1.
[7] D. A. Tenne, A. K. Farrar, C. M. Brooks, T. Heeg, J. Schubert, H. W. Jang, C. W. Bark, C. M. Folkman, C. B. Eom, D. G. Schlom, *Appl. Phys. Lett.* **2010**, *97*, 142901/1.
[8] M. Itoh, R. Wang, Y. Inaguma, T. Yamaguchi, Y. J. Shan, T. Nakamura, *Phys. Rev. Lett.* **1999**, *82*, 3540.
[9] A. K. Tagantsev, V. O. Sherman, K. F. Astafiev, J. Venkatesh, N. Setter, *J. Electroceram.* **2003**, *11*, 5.
[10] W. Zhong, D. Vanderbilt, *Phys. Rev. B* **1996**, *53*, 5047.
[11] N. A. Pertsev, A. K. Tagantsev, N. Setter, *Phys. Rev. B* **2000**, *61*, R825.
[12] N. A. Pertsev, A. G. Zembilgotov, A. K. Tagantsev, *Ferroelectrics* **1999**, *223*, 79.
[13] K. J. Choi, M. Biegalski, Y. L. Li, A. Sharan, J. Schubert, R. Uecker, P. Reiche, Y. B. Chen, X. Q. Pan, V. Gopalan, L. Q. Chen, D. G. Schlom, C. B. Eom, *Science* **2004**, *306*, 1005.
[14] G. A. Samara, P. S. Peercy, *Phys. Rev. B* **1973**, *7*, 1131.
[15] F. Gervais, W. Kress, *Phys. Rev. B* **1983**, *28*, 2962.
[16] P. D. Mitev, K. Hermansson, B. Montanari, K. Refson, *Phys. Rev. B* **2010**, *81*, 134303/1.
[17] T. S. Boescke, J. Mueller, D. Braeuhaus, U. Schroeder, U. Boettger, *Appl. Phys. Lett.* **2011**, *99*, 102903.
[18] J. Müller, U. Schröder, T. S. Böscke, I. Müller, U. Böttger, L. Wilde, J. Sundqvist, M. Lemberger, P. Kücher, T. Mikolajick, L. Frey, *J. Appl. Phys.* **2011**, *110*, 114113.
[19] J. Müller, T. S. Böscke, D. Bräuhaus, U. Schröder, U. Böttger, J. Sundqvist, P. Kücher, T. Mikolajick, L. Frey, *Appl. Phys. Lett.* **2011**, *99*, 112901.
[20] D. H. Triyoso, P. J. Tobin, B. E. White, Jr., *Appl. Phys. Lett.* **2006**, *89*, 132903.
[21] F. Chu, N. Setter, A. K. Tagantsev, *J. Appl. Phys.* **1993**, *74*, 5129.
[22] J. Wang, H. P. Li, R. Stevens, *J. Mater. Sci.* **1992**, *27*, 5397.
[23] R. C. Garvie, *J. Phys. Chem.* **1965**, *69*, 1238.
[24] N. Claussen, R. Wagner, L. J. Gauckler, G. Petzow, *J. Am. Ceram. Soc.* **1978**, *61*, 369.
[25] D. B. Marshall, M. R. Jarnes, J. R. Porter, *J. Am. Ceram. Soc.* **1989**, *72*, 218.
[26] E. H. Kisi, S. J. Kennedy, C. J. Howard, *J. Am. Ceram. Soc.* **1997**, *80*, 621.
[27] D. H. Looney, *US 2791758* **1957**.
[28] N. Setter, D. Damjanovic, L. Eng, G. Fox, S. Gevorgian, S. Hong, A. Kingon, H. Kohlstedt, N. Y. Park, G. B. Stephenson, I. Stolitchnov, A. K. Taganstev, D. V. Taylor, T. Yamada, S. Streiffer, *J. Appl. Phys.* **2006**, *100*, 51606.
[29] S. Y. Wu, *IEEE Trans. Electron Devices* **1974**, *ED-21*, 499.
[30] J. Hoffman, X. Pan, J. W. Reiner, F. J. Walker, J. P. Han, C. H. Ahn, *Adv. Mater.* **2010**, *22*, 2957.
[31] J. F. Scott, *Science* **2007**, *315*, 954.
[32] S. Salahuddin, S. Datta, *Nano Lett.* **2008**, *8*, 405.
[33] V. V. Zhirnov, R. K. Cavin, *Nat. Nanotechnol.* **2008**, *3*, 77.
[34] R. Meyer, R. Waser, K. Prume, T. Schmitz, S. Tiedke, *Appl. Phys. Lett.* **2005**, *86*, 142907.